Supplement of Atmos. Chem. Phys., 19, 4917–4931, 2019
https://doi.org/10.5194/acp-19-4917-2019-supplement

Atmospheric Chemistry and Physics
Open Access
EGU

Supplement of

pH-dependent production of molecular chlorine, bromine, and iodine from frozen saline surfaces

John W. Halfacre et al.

Correspondence to: John W. Halfacre (halfacre@ius.edu)

2. Methods

2.1 Materials

Acetic acid/acetate and bisulfate/sulfate buffer concentrations were 20 mM (10 mM of each acid and conjugate base). This concentration was chosen as a compromise between using as little buffer as possible and enough buffer to ensure adequate buffering ability, as buffer capacity rapidly decreases as constituent species concentrations approach the acid K_a value. The halide concentrations from our salt water solutions were Cl^- 500mM, Br^- 0.72mM, and I^- 1.9×10^{-3} mM.

Given that the buffer concentration is comparable to or exceeds halide ion concentrations, there is a question of whether buffer composition may change over time due to the volatility of acetic acid (Henry's Law constant of 400 M/atm), or because of buffer-constituent reactions with OH (concentration of 100 mM) that may compete with reactions between OH and halides. Here we present these potential reactions, associated rate constants, and calculate the potential for artifacts due to the presence of the buffer.

$\cdot OH + I^- \rightarrow HOI^-$	$k = 1.1 \times 10^{10}$ M^{-1} sec^{-1} (Buxton et al., 1988)
$\cdot OH + Br^- \rightarrow HOBr^-$	$k = 1.1 \times 10^{10}$ M^{-1} sec^{-1} (Zehavi and Rabani, 1972)
$\cdot OH + Cl^- \rightarrow HOCl^-$	$k = 3.0 \times 10^{9}$ M^{-1} sec^{-1} (Grigor'ev et al., 1987)
$CH_3CO_2H + \cdot OH \rightarrow H_2O + \cdot CH_2CO_2H$	$k = 9.2 \times 10^{6}$ M^{-1} sec^{-1} (Thomas, 1965)
$\cdot OH + HSO_4^- \rightarrow H_2O + SO_4^{\cdot -}$	$k = 4.7 \times 10^{5}$ M^{-1} sec^{-1} (Jiang et al., 1992)
$Cl^- + SO_4^{\cdot -} \rightarrow Cl\cdot + SO_4^{2-}$	$k = 2.6 \times 10^{8}$ M^{-1} sec^{-1} (Padmaja et al., 1993)
$Br^- + SO_4^{\cdot -} \rightarrow SO_4^{2-} + Br\cdot$	$k = 3.5 \times 10^{9}$ M^{-1} sec^{-1} (Redpath and Willson, 1975)

Using these aqueous rate constants and the pre-freezing concentrations of species (above and in main text Sect. 2.1), we find the following relative rates of OH reactions with halides, compared to OH reactions with buffer constituents:

$\frac{\frac{d[X^-]}{dt}}{\frac{d[HSO_4^-]}{dt}} = 3.6 \times 10^5, 1.7 \times 10^3,$ and 4.4 for Cl^-, Br^-, and I^-, respectively.

$\frac{\frac{d[X^-]}{dt}}{\frac{d[CH3CO2H]}{dt}} = 1.8 \times 10^4, 8.6 \times 10^1, 2.3 \times 10^{-1}$ for Cl^-, Br^-, and I^-, respectively.

It is clear based on these relative rates of production that, assuming OH + HSO_4^- is rate limiting, sulfate radical production would contribute only minorly to Br^- and Cl^- oxidation in our experiments, i.e., less than 0.1% of that from OH-halide oxidation. No analogous rate constant could be found for I^- reaction with the sulfate radical anion, and so

it is unclear the extent to which I^- oxidation (and subsequent I_2 formation) may be impacted by formation of the sulfate radical. The oxidation of acetic acid has no impact on our experiments to our knowledge. While it might decrease the OH radical concentration, this would not impact our study of the relative rates of halide oxidation by OH. This is further supported by the fact that the pH measurements before and after experiments were statistically identical (indicating no significant depletion of either buffer species throughout the experiment, and consequently, no significant depletion of OH by reactions with either buffer species).

2.2 Flow tube

Reaction photochemistry was achieved using six UVA-340 solar simulator lamps (Q-Labs, 295 – 400 nm with maximum wattage at 340 nm, irradiance spectrum in Fig. S1). These lamps were installed in the experiment box (two on each side, except bottom). Each side was lined with reflective Mylar sheets to evenly irradiate the flow tube when the lamps were powered.

2.3 CIMS

Experiments utilizing the bisulfate/sulfate buffer (IO3-5, IO8, SW3-5, SW8, and CL1) sometimes exhibited cyclical CIMS signal changes for Br_2 (*m/z* 285, 287, 291), IBr (*m/z* 333, 335) with no attributable cause. These signal changes occurred seemingly at random and to varying extents. In Fig. S2a, Experiment IO4 (pH = 1.7, includes H_2O_2) demonstrates the most extreme example of this behaviour that almost appears to affect the analysis. First at t = -3, the Br_2 rises briefly before falling. Then at t=2, the Br_2 signal begins to resemble a sine wave. All data beyond t=2 is not considered for this specific experiment. In Fig S2b, the effect during Experiment SW5 (pH = 1.7, includes H_2O_2) is more muted, beginning at approximately t = -6 for IBr and Br_2. As represented by these figures, this behaviour being farther away from our periods of integration is typical of the remaining experiments. Because these signal changes occurred outside of the experimental periods analyzed (i.e., before irradiation, and after O_3 had been active for one hour), they are therefore not believed to affect our results and their interpretation.

3 Results and Discussion

3.1 Dark reaction production of I_2

In cases without OH precursors at pH < 2, significant photochemical I_2 production still occurs (integrated production of 14 ± 10 nmol for IO8, and 6.0 ± 2.0 nmol for SW8), while Br_2 and Cl_2 concentrations remain below limits of detection (consistent with Abbatt et al., (2010), in which no Br_2 was observed without an OH-precursor) (Table 2, main text). This production likely stems from the mechanisms outlined by Kim et al. (2016) (R13-14, R10-R12), discussed in the Sect. 1. As discussed in Sect. 3.1, H_2O_2 or NO_2^- can react directly with I^-, thereby reducing the available [I^-] for photochemical OH oxidation when pH < 2. When H_2O_2 was the oxidant, integrated I_2 production amounts were found to be ≤ 0.82 nmol (IO4, IO5, and SW5), likely due to this initial dark depletion. When instead NO_2^- is used (as in IO3 and SW3), initial amounts of I_2 on flowtube connection to CIMS were less than when H_2O_2 was used (Table S1, Fig. S3). To estimate how much I^- may have been lost from our frozen sample by these dark mechanisms, we convert the integrated I_2 production amounts from Table S1 to I^- (by multiplying by 2) and subtract from the maximum possible moles of I^- in our samples (0.0800 L * 1.6 x 10^{-6} M = 1.28 x 10^{-7} moles I^-). For the samples that use hydrogen peroxide, as little as 36– 91% of I^- is available for reaction, while 94-97% remain when using NO_2^-. However, it is certain that not all of the I_2 produced by this mechanism went into the CIMS by the nature of having to break the flow tube seal in order to connect it to the CIMS. Therefore, these are only estimates that could be affected by the length of time the tube is open to the environment and not connected to the CIMS, or sealed shut.

3.2 Hydroxyl radical-induced halogen production

3.2.1 pH ≈ 4.7

Considering the values of I_2 production from Table 2 (main text), IO2, appears to have produced ~10 times less I_2 based on the chosen period of integration. It was noted that I_2 appeared to already be present within the flow tube on connecting the flow tube to the CIMS (Fig. S4). The integrated sum of I_2 released on connection of the flow tube to the CIMS until stabilization was 0.8 (± 0.1) nmol, corresponding to approximately 0.5% of the total 152 nmol I^- available for reaction from the Instant Ocean solution (Table S1). This production could possibly be induced by the dark reactions described in Sect. 3.1. However, the experiment otherwise eventually produces the same qualitative features as the other three experiments after light activation (Fig. S4). If instead the limits of integration are chosen

starting when the I_2 signal begins rising (i.e., during a period that qualitatively resembles the other experiments), the integrated I_2 production amounts (1.1 ± 0.6 nmol) more closely approaches analogous experiments (IO1, SW1, SW2). The apparent photochemical integrated Br_2 sum of 0.034 ± 0.003 nmol (Table 2) represents a real signal just above the limit of detection (1.8 ± 0.4 pmol mol^{-1}), but this baseline signal does not change on addition of light (Fig. 3a). In addition, the integration method used likely interpolated missing data for time periods in which incorrect isotope ratios between *m/z* 285 and 287 were observed, thereby overestimating the integrated yield. This signal remains below limits of quantitation and should not be considered further. Cl_2 concentrations remained below limits of detection for experiment IO2.

In most cases, it was also found that extending limits of integration beyond 1 h after addition of O_3 did not produce I_2 in amounts that exhausted the supply of I^-. In an example experiment (IO2, Fig. S5), the limits of integration were extended to t = 15 hours after the initiation of lights. While the signal appeared to stabilize below the I_2 LOD of 9 pmol mol^{-1}, the calculated I_2 production amount of 70 nmol for this extended integration period only accounts for 46% of the 152 total nmol of I^- available. When repeated for the other experiments at pH = 4.7, it is found that at least 16% of the original I^- remains unreacted after similarly extended limits of integration. This suggests that all of the I^- in our frozen samples may not be completely excluded to the disordered interface, and may exist within the ice bulk or inaccessible brine channels throughout the ice, and that differences in integration production amounts can originate from differences in I^- distribution during freezing (Bartels-Rausch et al., 2014; Malley et al., 2018).

3.2.2 pH≤ 2

At low pH (~2), and with H_2O_2 as our OH precursor, we noted a large outflux of I_2 on connecting the flow tube to the CIMS. Br_2 production was readily observed in the presence of light, and enhanced when the samples were exposed to O_3, as in Fig 2b. However, experiment SW3 (Fig. S5), which was performed with NO_2^- as the hydroxyl radical precursor, exhibited photochemical I_2 production on the introduction of radiation. Only after the introduction of O_3 was Br_2 observed (under proper isotope ratios).

3.3 Effects of O_3 on halogen production

As discussed in the main text, HOX compounds were observed when O_3 was added to the flow tube. With regard to the extent to which it affects our observed signal, we believe volatile organic compounds, such as aldehydes

and ketones, that may form gas phase HX could originate from our cylinder of zero air. However, we believe this source would be effectively scrubbed by our activated charcoal trap (Fig. 1), mitigating any gas phase production of HX. There also exists organic matter in the condensed phase, averaging 70 mg/L in each Instant Ocean sample (Sect. 2 of the main text). This carbon-matter is presumably uncharged and would freeze throughout the formed ice (i.e., no freeze concentration effect), therefore making only a small fraction of the total carbon available at the frozen surface for reaction.

If any of this solution-based carbon were involved in making HX, it would be expected that the SW and IO experiments produce different amounts of $IOHX^-$, given that the SW experiments were found to average ~5 mg/L of dissolved organic matter. However, there is no difference in the signal changes between corresponding SW and IO experiments (Figs. 3-4, S6). Therefore, we believe the primary source of $IOHX^-$ in the CIMS is, indeed, HOX formed in the flow tube.

References

Abbatt, J., Oldridge, N., Symington, A., Chukalovskiy, V., McWhinney, R. D., Sjostedt, S. and Cox, R. A.: Release of Gas-Phase Halogens by Photolytic Generation of OH in Frozen Halide−Nitrate Solutions: An Active Halogen Formation Mechanism?, J. Phys. Chem. A, 114(23), 6527–6533, doi:10.1021/jp102072t, 2010.

Bartels-Rausch, T., Jacobi, H.-W., Kahan, T. F., Thomas, J. L., Thomson, E. S., Abbatt, J. P. D., Ammann, M., Blackford, J. R., Bluhm, H., Boxe, C., Domine, F., Frey, M. M., Gladich, I., Guzmán, M. I., Heger, D., Huthwelker, T., Klán, P., Kuhs, W. F., Kuo, M. H., Maus, S., Moussa, S. G., McNeill, V. F., Newberg, J. T., Pettersson, J. B. C., Roeselová, M. and Sodeau, J. R.: A review of air–ice chemical and physical interactions (AICI): liquids, quasi-liquids, and solids in snow, Atmos Chem Phys, 14(3), 1587–1633, doi:10.5194/acp-14-1587-2014, 2014.

Buxton, G. V., Greenstock, C. L., Helman, W. P. and Ross, A. B.: Critical Review of rate constants for reactions of hydrated electrons, hydrogen atoms and hydroxyl radicals (·OH/·O^- in Aqueous Solution, J. Phys. Chem. Ref. Data, 17(2), 513–886, doi:10.1063/1.555805, 1988.

Grigor'ev, A. E., Makarov, I. E. and Pikaev, A. K.: Formation of Cl_2^- in the bulk of solution during radiolysis of concentrated aqueous solutions of chlorides, Khimiya Vysok. Ehnergij, 21(2), 123–126, 1987.

Jiang, P.-Y., Katsumura, Y., Nagaishi, R., Domae, M., Ishikawa, K., Ishigure, K. and Yoshida, Y.: Pulse radiolysis study of concentrated sulfuric acid solutions. Formation mechanism, yield and reactivity of sulfate radicals, J. Chem. Soc. Faraday Trans., 88(12), 1653–1658, doi:10.1039/FT9928801653, 1992.

Malley, P. P. A., Chakraborty, S. and Kahan, T. F.: Physical Characterization of Frozen Saltwater Solutions Using Raman Microscopy, ACS Earth Space Chem., doi:10.1021/acsearthspacechem.8b00045, 2018.

Padmaja, S., Neta, P. and Huie, R. E.: Rate constants for some reactions of inorganic radicals with inorganic ions. Temperature and solvent dependence, Int. J. Chem. Kinet., 25(6), 445–455, doi:10.1002/kin.550250604, 1993.

Redpath, J. L. and Willson, R. L.: Chain Reactions and Radiosensitization: Model Enzyme Studies, Int. J. Radiat. Biol. Relat. Stud. Phys. Chem. Med., 27(4), 389–398, doi:10.1080/09553007514550361, 1975.

Thomas, J. K.: Rates of reaction of the hydroxyl radical, Trans. Faraday Soc., 61(0), 702–707, doi:10.1039/TF9656100702, 1965.

Zehavi, D. and Rabani, J.: Oxidation of aqueous bromide ions by hydroxyl radicals. Pulse radiolytic investigation, J. Phys. Chem., 76(3), 312–319, doi:10.1021/j100647a006, 1972.

Tables

Table S1: Integrated I_2 production amounts prior to irradiation or addition of O_3 from low pH experiments involving samples with an OH precursor. The period of integration was chosen to be immediately after connection of flow tube to the CIMS until sample was irradiated. Average LODs for I_2 across experiments was 9 ± 2 pmol mol^{-1}. "IO#" represents samples composed of Instant Ocean, and "SW#" represents "saltwater" samples, composed of reagent salts.

Experiment	Oxidant	pH	I_2 produced (nmol)	Integration time (hours)	Estimated Percent of I^- remaining for reaction
IO3	NO_2^-	2.0	4.0(±0.1)	0.55	93.7
SW4	NO_2^-	2.2	2.5(±0.1)	0.43	96.1
SW3	NO_2^-	1.8	2.0(±0.1)	0.83	96.8
IO4	H_2O_2	1.7	41(±14)	7.28	36.2
IO5	H_2O_2	1.7	5.7(±1.9)	2.92	91.1
SW5	H_2O_2	1.8	41(±14)	4.95	35.5

Table S2: Integrated I_2 produced from pH = 4.7 experiments involving samples with an OH precursor. The period of integration begins at sample irradiation and extends past the limits of analysis used in the main text. Average LODs for I_2 across experiments was 9 ± 2 pmol mol^{-1}. "IO#" represents samples composed of Instant Ocean, and "SW#" represents "saltwater" samples, composed of reagent salts.

Experiment	Oxidant	pH	I_2 produced (nmol)	Integration time (hours)	Estimated Percent of I^- remaining for reaction
IO1	H_2O_2	4.7	31(±10)	30	59
IO2	H_2O_2	4.7	35(±20)	15	54
SW1	H_2O_2	4.7	63(±23)	23	17
SW2	H_2O_2	4.5	63(±20)	17	16

Figures

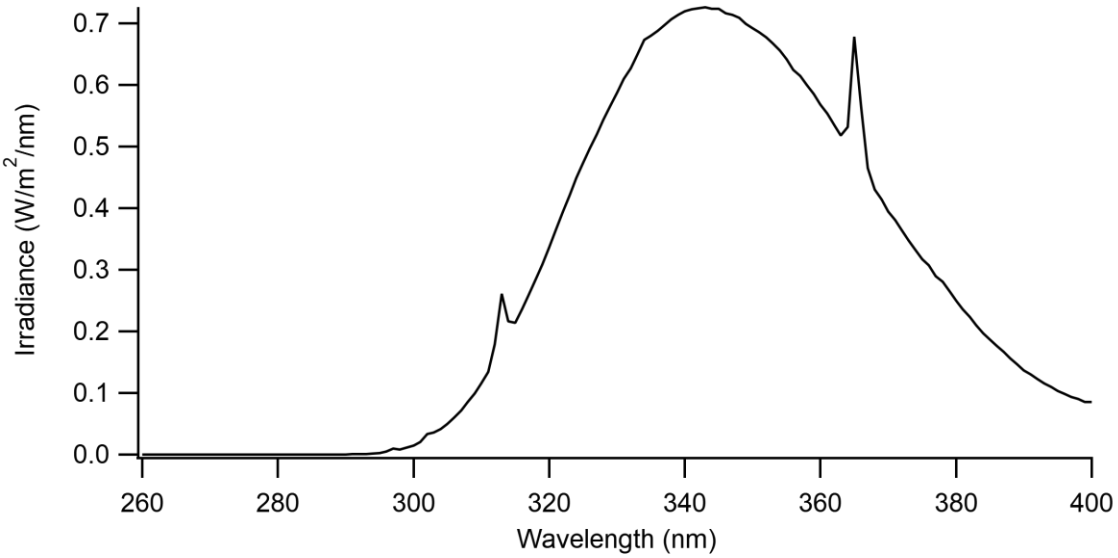

Figure S1: Irradiance spectrum for the Q-Lab UVA 340 Lamps, reproduced with permission from Q-Lab Corporation Technical Bulletin LU-8052 – "SPD for QUV UVA-340."

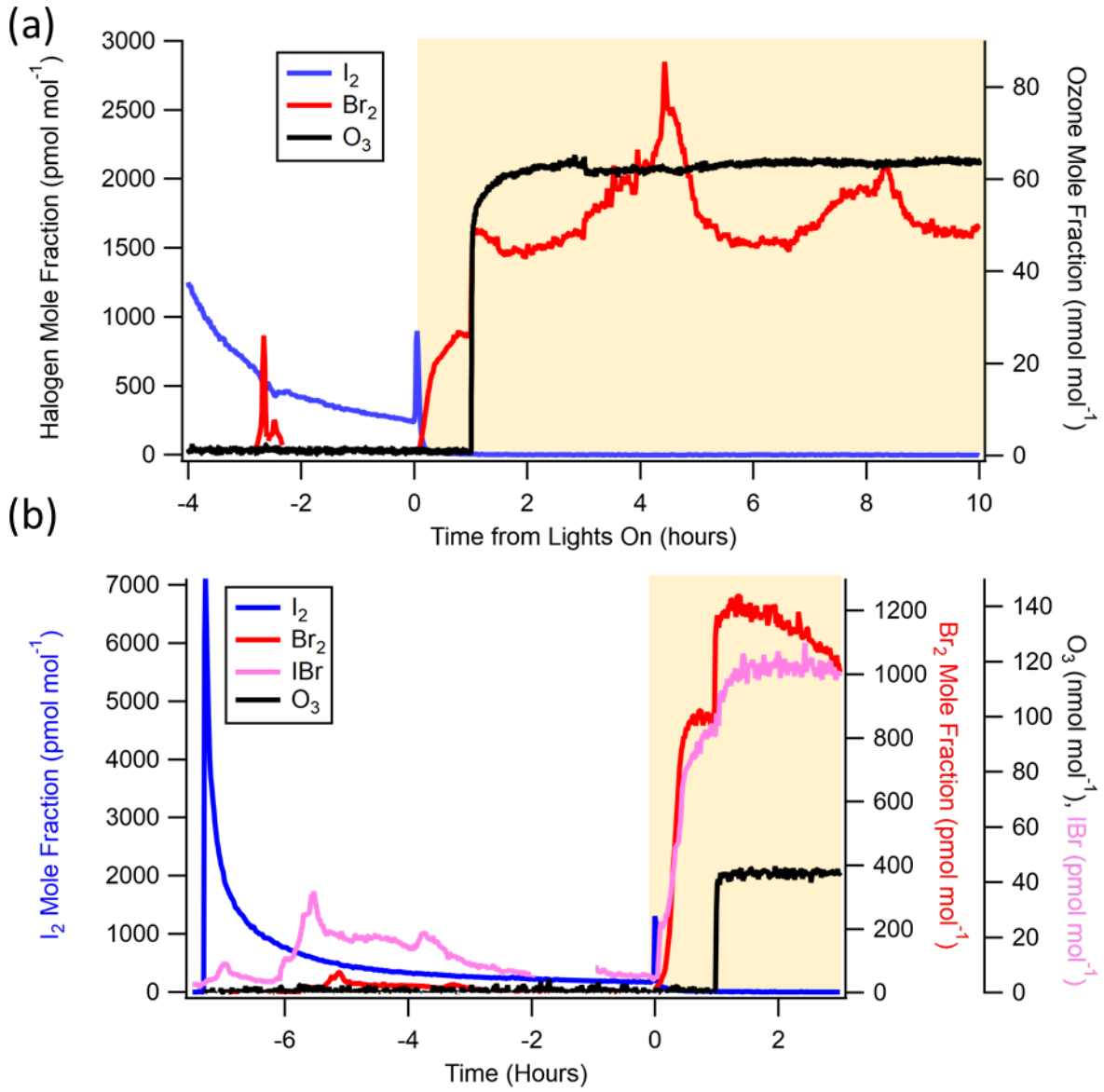

Figure S2: a) Experiment IO4 (pH < 2, includes H_2O_2) time series demonstrating cyclical increases in signal Br_2 signals, especially at t= -3 and beginning again at t = 2. Period of analysis in main text includes t = 0 until t=2. b) Experiment SW5 (pH < 2, includes H_2O_2) time series demonstrating cyclical signals for IBr and Br_2, beginning predominately at t = -6 until shortly before t = 0.

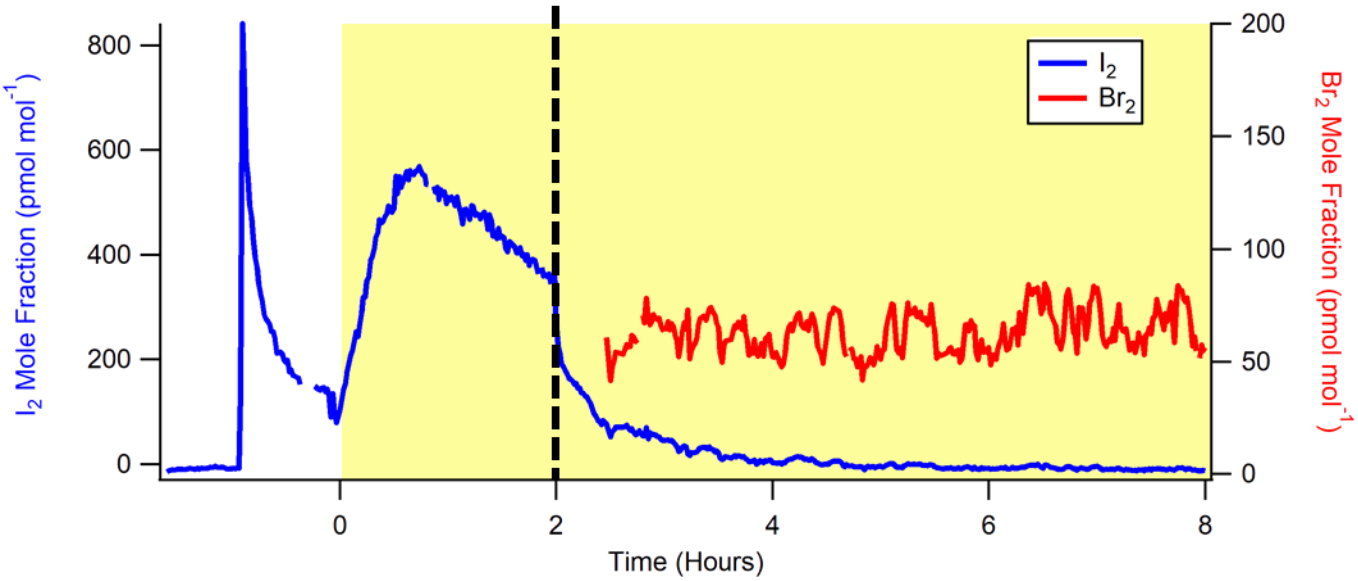

208

209 Figure S3: Experiment SW3, using synthetic seawater at pH = 1.8, in which NO_2^- acted as our hydroxyl
210 radical precursor. Ozone was introduced at hour two (indicated by dashed vertical line), coincident with
211 the I_2 concentration decrease. Br_2 data filtered based on correctness of isotope ratios between *m/z* 285 and
212 287 (IBrBr).

213

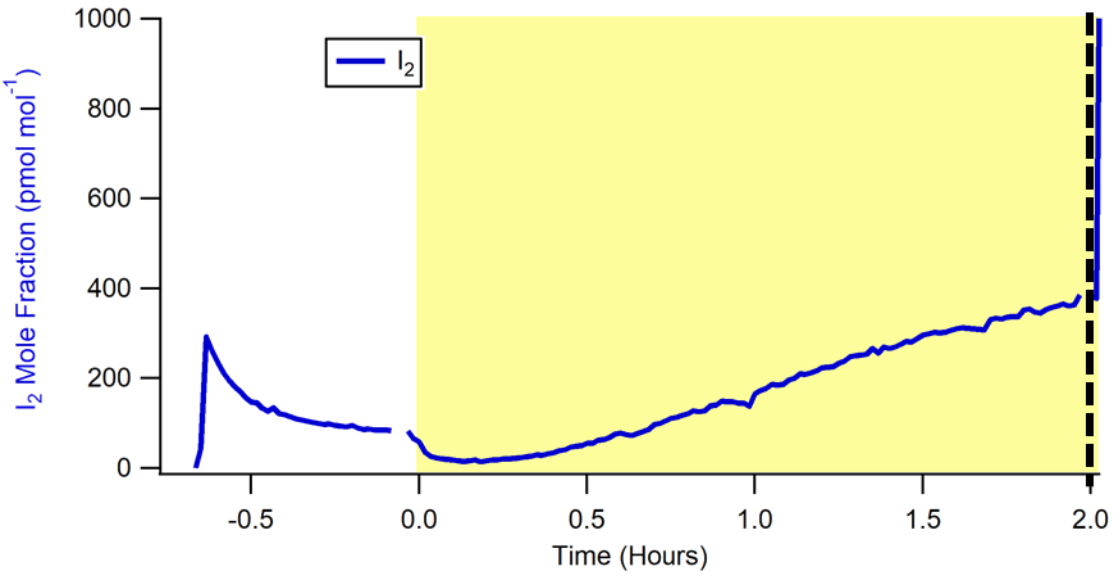

Figure S4: Experimental timeseries for experiment IO2. The key difference between this experiment and others at pH ~4.68 is that there was some initial I_2 present when the flow tube was connected to the CIMS. On activating the lights, these concentrations lowered, before ultimately rising due to OH-induced I_2 production. Beginning the integration when the signal begins rising leads to similar production values as those experiments without this initial I_2 present. Vertical dashed line represents when O_3 was introduced to the system.

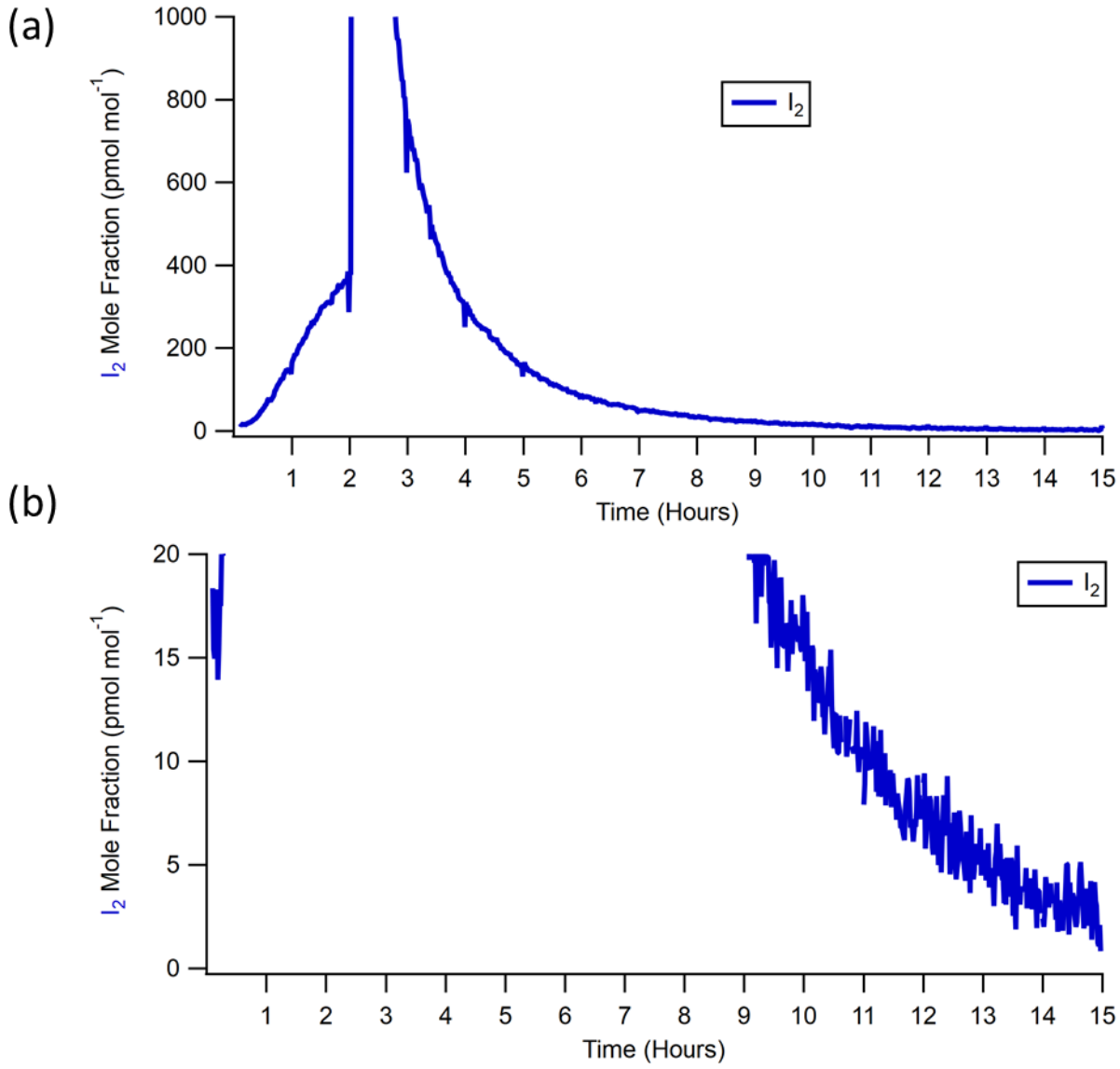

Figure S5: Iodine time series from experiment IO2, using Instant Ocean at pH = 4.7, in which H_2O_2 acted as our hydroxyl radical precursor. The x-axis begins on light introduction to the flow tube, while ozone was introduced at hour two as indicated by the sudden increase in signal. (a) The time series signal rapidly increases at t=2 coincident with the addition of 60 nmol mol^{-1} of O_3, and then returns to baseline by hour 13. (b) Zoomed in version of the same plot

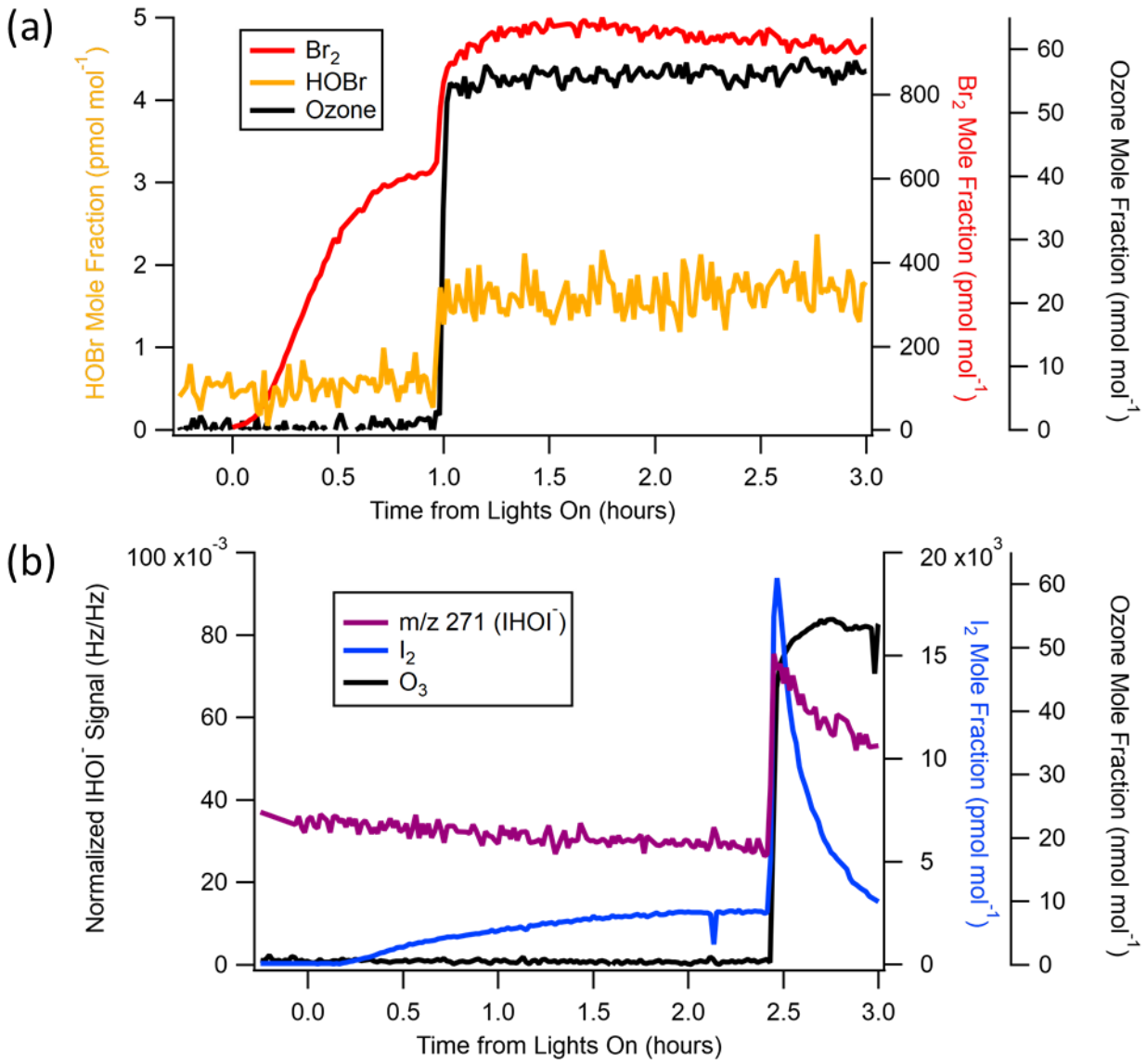

Figure S6: a) Experiment IO5, using Instant Ocean at pH = 1.7, in which H_2O_2 acted as our hydroxyl radical precursor (analogous to SW5, Fig. 4). Comparison of Br_2 mole fractions to HOBr. Note that the HOBr signal should be used only for qualitative purposes as its identity could not be confirmed using isotopic ratios with *m/z* 223 due to its relatively large background signal. Br_2 data filtered based on correctness of isotope ratios between *m/z* 285 and 287 ($IBrBr^-$). b) Experiment SW2 (analogous to IO2, Fig. 3) showing effect of O_3 on I_2 and HOI.